From the sparse to the statistical limit of intramolecular vibrational redistribution in vibrational predissociation: ArCl2 as an example

Octavio Roncero, David Caloto, Kenneth C. Janda, and Nadine Halberstadt

Citation: J. Chem. Phys. **107**, 1406 (1997); doi: 10.1063/1.474495
View online: http://dx.doi.org/10.1063/1.474495
View Table of Contents: http://jcp.aip.org/resource/1/JCPSA6/v107/i5
Published by the American Institute of Physics.

From the sparse to the statistical limit of intramolecular vibrational redistribution in vibrational predissociation: $ArCl_2$ as an example

Octavio Roncero and David Caloto
Instituto de Matemáticas y Física Fundamental, C.S.I.C. Serrano 123, 28006 Madrid, Spain

Kenneth C. Janda
Department of Chemistry and ISIS, University of California, Irvine, California 92715

Nadine Halberstadt
LCAR-IRSAMC, Université Paul Sabatier et CNRS, 31062 Toulouse Cedex, France

(Received 17 March 1997; accepted 25 April 1997)

The dynamics of intramolecular vibrational relaxation (IVR) for $ArCl_2$ are examined for a wide range of vibrational and rotational excitation. In order to describe the IVR more efficiently, and characterize it more quantitatively, we propose a refinement of the traditional Bixon-Jortner description in which the active states are prediagonalized to simplify the coupling scheme that must be considered. This allows for an explicit determination of the average density of states and average coupling strength for each initial excitation. We find that the IVR dynamics proceed from the sparse regime for $v=11$, for which the first open dissociation channel corresponds to the loss of two Cl_2 quanta, to the intermediate-dense regime for $v=25$ which dissociates by the loss of 4 quanta. We find that over this range the increase in the density of states is less important than the increase in the coupling strength. For $v=18$ we examine the effect of rotation in considerable detail. Initial states that couple *via* a manifold of 6000 channels can be considered since the calculation is performed on a parallel computer. The effect of increasing J, the total angular momentum excitation, is found to be less than that of increasing K, the degree of rotation about the van der Waals bond. This means that the main effect is not simply an increase of the available density of states due to Coriolis coupling. Understanding the details of IVR in a relatively simple system like $ArCl_2$ should help us understand the dynamics of more complicated molecules. In particular, the case of ArI_2 is discussed. © *1997 American Institute of Physics.* [S0021-9606(97)02829-8]

I. INTRODUCTION

van der Waals clusters provide interesting model systems for characterizing intramolecular vibrational redistribution (IVR). The molecule can be excited to a well defined state, which undergoes IVR and this eventually leads to dissociation of the weak van der Waals bond. Triatomic molecules are especially interesting because the IVR dynamics can be completely characterized by both experiment and theory. For rare gas-halogen species, for example, the dynamics can be experimentally studied in both the frequency[1–4] and time[5,6] domains. The fact that IVR dynamics could occur in such a simple molecule was first demonstrated for $ArCl_2$,[7] for which vibrational predissociation (VP) occurs through sequential loss of two quanta of the chlorine stretch to the van der Waals manifold. Since the result of the first vibrational transfer is the production of a highly vibrationally excited van der Waals mode, the final dissociation step leads to a very complicated product rotational distribution. This is in contrast to the dynamics of $HeCl_2$ and $NeCl_2$ (Refs. 8–11) for which $\Delta v=-2$ dissociation occurs by direct coupling to the continuum manifold of states and for which the product rotational distribution were much simpler. Quantum calculations[12–15] for $ArCl_2$ confirmed that the IVR model of sequential coupling is correct. Optical excitation prepares a ''bright'' state corresponding to the ground van der Waals level of a given chlorine vibrational state v. This bright state first couples to a ''dark'' state that corresponds to a highly excited van der Waals level associated with the chlorine $v-1$ state. This dark state then couples to the $v-2$ continuum of dissociative states. Since a different dark state couples to each possible bright state, due to the chlorine anharmonicity, the final rotational state distribution is different for each initial bright state. Similar IVR dynamics have recently been observed for very high vibrational levels of $HeBr_2$ which decay by sequential $\Delta v=-2$ when the $\Delta v=-1$ channel is closed. The erratic dependence of the measured lifetime on the initial vibrational quantum number[16] has been reproduced by recent calculations.[17]

For ArI_2 vibrational predissociation competes with electronic predissociation in the $v=16$ to 24 vibrational excitation range.[1,18,5,4] From intensity measurements it has been deduced that VP rates increase monotonically with vibrational excitation.[1,20] Recent measurements[4] have confirmed this smooth variation of the VP rate with v, based on a very similar linewidth for the ground and the first excited van der Waals states. In this vibrational range VP occurs via the transfer of three quanta from the I_2 stretch to the van der Waals degrees of freedom and the IVR model is appropriate.[21–23] For the VP dynamics to have the monotonic dependence on energy observed by Klemperer *et al.*, the IVR dynamics must occur in the statistical limit for which a large number of doorway states are coupled to the bright state. If only a few dark states were coupled to the bright state, i.e.,

inthe sparse IVR regime, then erratic dynamics such as that observed for $ArCl_2$ and $HeBr_2$ would also have been observed for ArI_2. The statistical limit of IVR has been traditionally attributed only to large molecules,[24,25] so the possibility that it applies to ArI_2 is quite surprising.

In this paper we explore the possibility that the statistical limit of IVR can occur for a triatomic van der Waals molecule. We focus on $ArCl_2$ since it is more amenable to exact quantum calculations. This also allows us to check the validity of statistical models such as the Bixon-Jortner model[24] and could also be compared with the random matrix model.[26–28] In the former model, the levels and widths of the dark states are assumed to be uniform, while in the latter case they are chosen at random from a distribution function. Applicable distribution functions have been discussed for molecular, atomic[29] and nuclear problems.[30]

We examine how vibrational and rotational excitation cause the dynamics to shift from the sparse to the statistical limit. The density of doorway states of $ArCl_2$ increases rapidly with rotational[23] and vibrational excitation. The density of states is proportional to $(2J+1)$ for rotational excitation because of Coriolis coupling. In this respect the behavior of $ArCl_2$ and ArI_2 should be quite similar. The change in the dynamics with vibrational excitation is faster for $ArCl_2$ than for ArI_2 because of the larger anharmonicity. One consequence of this large anharmonicity is that the number of chlorine vibrational quanta needed to dissociate the van der Waals bond changes rapidly with v. We study the VP dynamics for initial excitation to $v=18$, 22 and 25, for which 3, 4 and 5 vibrational quanta, respectively, are required for dissociation. For $v=18$ we examine the effect of rotational excitation up to $J=15$. For several values of J, we also examine the effect of changing the orientation of rotation with respect to the molecular axes. Although these dynamical processes have not been observed in this regime for $ArCl_2$ because of competition from electronic predissociation, these calculations serve as a model system for understanding the dynamics of ArI_2. Comparable calculations for ArI_2 are quite difficult. Only recently have $J \gg 0$ calculations been performed.[31] However, without including the effect of orientation, the statistical limit was not reached.

The organization of the paper is as follows. Section II gives a brief review of the usual treatment for radiationless processes. Particular attention is paid to the case of independent resonances. This case is valid when many resonances participate in the dynamics. Next, simplifications are presented which yield a simple model for classifying different IVR regimes. This model is analogous to previous models,[24,25,32,33] with the advantage of being completely analytical. In section III the details of the quantum mechanical time-dependent calculations are presented. The angular coordinates are described using a combination of a Discrete Variable Representation (DVR) and a Finite Basis representation (FBR). In section IV numerical results are presented and analyzed in terms of the analytical models described in section II. Finally, section V is devoted to conclusions.

II. CHARACTERIZATION OF IVR REGIMES

Radiationless transitions are often described in terms of the eigenstates of a zero-order Hamiltonian, H_0, which are coupled by $V=H-H_0$ where H is the complete Hamiltonian. The eigenstates of H_0 can be either discrete, $\phi_i^{(0)}$, or continuum, $\phi_{\alpha,E}^{(0)}$ states, and provide a complete basis for the description of the system. The continuum states can correspond to photon emission or to dissociation: the subscript α is a collective index which describes the asymptotic states of the system. For the case under study, dissociation is much faster than emission and hereafter we shall only refer to the possibility of dissociation without loss of generality. Also, for this case it is a good approximation to assume that the initial state, ϕ_0, created by photo-excitation can be described using only the zero-order discrete states[14]

$$\phi_0=\sum_k a_k^{(0)}\phi_k^{(0)}. \tag{1}$$

The absorption spectrum can then be expressed as[23],

$$\sigma(E)\propto\sum_\alpha \left|\sum_k a_k^{(0)*}\sum_j \langle\phi_k^{(0)}|G(E)|\phi_j^{(0)}\rangle \times\langle\phi_j^{(0)}|V|\phi_{\alpha,E}^{(0)}\rangle\right|^2. \tag{2}$$

$\langle\phi_k^{(0)}|G(E)|\phi_j^{(0)}\rangle$ are the resolvent operator matrix elements given by

$$\begin{pmatrix} G_{11}^{(0)}(E) & G_{12}^{(0)}(E) & \cdots \\ G_{21}^{(0)}(E) & G_{22}^{(0)}(E) & \cdots \\ \vdots & \vdots & \ddots \end{pmatrix} = \begin{pmatrix} E-E_1^{(0)}-\Delta_1^{(0)}+i\Gamma_1^{(0)} & -V_{12}^{(0)}-\Delta_{12}^{(0)}+i\Gamma_{12}^{(0)} & \cdots \\ -V_{21}^{(0)}-\Delta_{21}^{(0)}+i\Gamma_{21}^{(0)} & E-E_2^{(0)}-\Delta_2^{(0)}+i\Gamma_2^{(0)} & \cdots \\ \vdots & \vdots & \ddots \end{pmatrix}^{-1}. \tag{3}$$

$\Gamma_{kj}^{(0)}=\pi\langle\phi_k^{(0)}|V|\phi_{a,E}^{(0)}\rangle\langle\phi_j^{(0)}|V|\phi_{a,E}^{(0)}\rangle^*$ and $\Delta_{kj}^{(0)}$ are indirect couplings between the zero-order bound states due to their dissociation to the same continua.[34,28,14] To invert the matrix on the right-handside of Eq.(3) it is convenient to first diagonalize it by an orthogonal transformation, **T**, yielding the ω_k eigenvalues. The population of the initial state as a function of time is then given by[35]

$$P_b(t)=\left|\sum_k \sum_j a_k^{(0)*} a_j^{(0)} \sum_l (\mathbf{T}^{-1})_{kl} e^{-i\omega_l t/\hbar} (\mathbf{T})_{lj}\right|^2. \tag{4}$$

Using these expressions and a well chosen subset of the zero-order basis set results in a simplified model for describing the IVR dynamics. The energies and the couplings on the right hand side of Eq. (3) can be treated as parameters to fit experimental or theoretical results. This is a generalization of the analysis that was applied to the $\Delta v=-2$ dissociation of $ArCl_2$. In that case two zero-order discrete states were sufficient to accurately describe the absorption spectrum, the time evolution of zero-order bound states, and the dissociation probabilities.[14]

If Eqs. (1–4) are used directly in the fitting procedure, the results are very sensitive to the relative position of the zero-order states and their mutual couplings. For this reason it is convenient to construct a new basis set, hereafter referred to as first-order, in which the complete Hamiltonian is diagonalized in the discrete part of the basis set, since the continuum subspace has been assumed to be diagonal. In the pre-diagonalized basis the expressions for the initial state, the spectrum, and the time evolution of the population, remain quite similar to Eqs. (1), (2), and (4). The changes in the equations of the resolvent operator are more substantial. Eq. (3) becomes

$$\begin{pmatrix} G_{11}^{(1)}(E) & G_{12}^{(1)}(E) & \cdots \\ G_{21}^{(1)}(E) & G_{22}^{(1)}(E) & \cdots \\ \vdots & \vdots & \ddots \end{pmatrix} = \begin{pmatrix} E-E_1-\Delta_1+i\Gamma_1 & -\Delta_{12}+i\Gamma_{12} & \cdots \\ -\Delta_{21}+i\Gamma_{21} & E-E_2-\Delta_2+i\Gamma_2 & \cdots \\ \vdots & \vdots & \ddots \end{pmatrix}^{-1}. \tag{5}$$

In the prediagonalized basis the only coupling terms that remain in Eq. (5) result from indirect coupling of the bound states via the continuum. These coupling terms represent interferences[34,28,14] and can be positive or negative. When the number of states is large the coupling terms tend to cancel out[28] and can be neglected. The absorption spectrum then reduces to a collection of independent Lorentzians,

$$\sigma(E)\propto\sum_k \frac{\Gamma_k}{\pi}\frac{|a_k|^2}{(E-E_k)^2+\Gamma_k^2}. \tag{6}$$

The population of the bright state becomes

$$P_b(t)=\sum_k |a_k|^4 e^{-2\Gamma_k t/\hbar}+2\sum_k \sum_{k'>k} |a_k|^2|a_{k'}|^2 \times e^{-(\Gamma_k+\Gamma_{k'})t/\hbar}\cos(E_k-E_{k'})t/\hbar, \tag{7}$$

and the dissociation probability can be simply expressed as

$$P_d(t)=1-\sum_k |a_k|^2 e^{-2\Gamma_k t/\hbar}. \tag{8}$$

A useful classification of IVR regimes can be obtained by applying simplifying assumptions to the above equations. Bixon and Jortner[24] developed such a model corresponding to the zero-order basis set. They assumed that the initial state is coupled to an infinite number of equally spaced dark states. The dark states all have the same width, $\Gamma\equiv\Gamma_k$, and the same coupling V to the initial bright state.

Here we make similar assumptions, but work in the first-order basis set described above. We assume an infinite number of equidistant bound states with the same width Γ and with energies $E_k=k\Delta$ $(-\infty\leqslant k\leqslant\infty)$. The coefficients of the initial state in this basis are $a_k/a_0=V/(k\Delta-i\Gamma)$, where V is the coupling in the zero-order basis. This formulation is equivalent with that of Bixon and Jortner in most cases,[36] and provides the following simplified equation for the absorption spectrum:

$$\sigma(E)=\frac{B}{\pi A}\left\{\frac{(\Gamma^2-|V|^2)/\Gamma}{E^2+\Gamma^2}+\frac{\Gamma_{\mathrm{IVR}}}{E^2+4\Gamma^2}\left[\frac{e^{\pi\Gamma/\Delta}+e^{-\pi\Gamma/\Delta}}{e^{\pi\Gamma/\Delta}-e^{-\pi\Gamma/\Delta}}+\frac{1}{E}\frac{4\Gamma\,\sin 2\pi E/\Delta+E(e^{2\pi\Gamma/\Delta}-e^{-2\pi\Gamma/\Delta})}{e^{2\pi\Gamma/\Delta}+e^{-2\pi\Gamma/\Delta}-2\cos 2\pi E/\Delta}\right]\right\}, \tag{9}$$

where $\Gamma_{\mathrm{IVR}}=\pi|V|^2/\Delta$,

$$\begin{aligned} A&=\{\Gamma^2-|V|^2\}\{e^{2\pi\Gamma/\Delta}+e^{-2\pi\Gamma/\Delta}-2\}-\Gamma_{\mathrm{IVR}}\Gamma\{e^{-2\pi\Gamma/\Delta}-e^{2\pi\Gamma/\Delta}\},\\ B&=\Gamma^2\{e^{2\pi\Gamma/\Delta}+e^{-2\pi\Gamma/\Delta}-2\}, \end{aligned} \tag{10}$$

and the time dependence of the evolution of the initial state population,

$$P_b(t)=\frac{B^2}{A^2\Gamma^4}\frac{e^{-2\Gamma t/\hbar}}{e^{2\pi\Gamma/\Delta}+e^{-2\pi\Gamma/\Delta}-2}\{e^{2\pi\Gamma/\Delta}(\Gamma^2-|V|^2+\Gamma_{\mathrm{IVR}}\Gamma e^{-\Gamma T/\hbar})^2+e^{-2\pi\Gamma/\Delta}(\Gamma^2-|V|^2-\Gamma_{\mathrm{IVR}}\Gamma e^{\Gamma T/\hbar})^2 -2(\Gamma^2-|V|^2+\Gamma_{\mathrm{IVR}}\Gamma e^{-\Gamma T/\hbar})(\Gamma^2-|V|^2-\Gamma_{\mathrm{IVR}}\Gamma e^{\Gamma T/\hbar})\}, \tag{11}$$

with $T=t-2\pi\hbar n/\Delta$, n being the integer part of $t\Delta/2\pi\hbar$.

The qualitative nature of the functions $\sigma(E)$ and $P_b(t)$, as defined above, changes with the ratio Γ/Δ (see Figs. 1). This leads to a natural classification, as previously discussed,[24,25,32,33] of IVR dynamics.

(a) **Sparse regime,** ($\Gamma \ll \Delta$): In this regime the resonances are well separated. The initially populated bright state will usually interact with a single dark state, so that quantum phenomena such as recurrences are readily apparent. However, this means that the Γ_{kj} terms, neglected in the classification model, are usually important. For a detailed analysis of this regime, the simplifying assumptions made above should not be used and are not necessary.

(b) **Intermediate regime,** ($\Gamma \approx \Delta$): In this regime the resonances are mixed but have not completely lost their individual identity. This will be apparent in both the spectrum, in which nearby transitions will overlap with each other, and in the dynamics, which will exibit nonexponential decay with weak recurrences in the population of the initially excited states.

(c) **Statistical regime,** ($\Gamma \gg \Delta$): In this regime there are many closely spaced resonances that blend together to yield a quasi-Lorentzian excitation spectrum. As a consequence, the initial states lose their identity and decay irreversibly as a single exponential.

III. QUANTUM TIME-DEPENDENT DYNAMICS

The formalism used in this paper is based on that previously discussed in detail, except that overall rotation is explicitly included. Therefore, a brief review of the method is presented.

The Hamiltonian of a triatomic system using Jacobi coordinates is

$$H=-\frac{\hbar^2}{2m}\frac{\partial^2}{\partial R^2}+\frac{l^2}{2mR^2}-\frac{\hbar^2}{2\mu}\frac{\partial^2}{\partial r^2}+\frac{\mathbf{j}^2}{2\mu r^2}+V(r,R,\theta)+V_{BC}(r), \tag{12}$$

where $\mathbf{r}$ is the Cl_2 intramolecular distance, $\mathbf{R}$ goes from the Cl_2 center of mass to the Ar atom, and θ is the angle between these two vectors. The angular momentum operators, $\mathbf{j}$ and l, are associated with $\mathbf{r}$ and $\mathbf{R}$, respectively. $V_{BC}(r)$ is the potential for the vibrational coordinate of the diatomic and $V(r,R,\theta)$ the van der Waals interaction potential.

In a body-fixed frame chosen such that the z-axis lies along the $\mathbf{R}$ vector and all three atoms lie in the x-z plane, the total wavepacket is expanded as

$$\Psi^{JM}(\mathbf{R},\mathbf{r},t)=\sum_{\Omega\geqslant 0}^{J}\sum_{v} W^{Jp}_{M\Omega}(\phi_R,\theta_R,\phi)\times\Phi^{JM}_{\Omega,v}(R,\theta,t)\chi_v(r). \tag{13}$$

ϕ_R, θ_R, and ϕ are the Euler angles specifying the orientation of the body-fixed frame. The $W^{Jp}_{M\Omega}$ functions are linear combinations of Wigner rotation matrices such that the parity under inversion of all coordinates, p, is well defined

$$W^{Jp}_{M\Omega}(\phi_R,\theta_R,\phi)=\sqrt{\frac{2J+1}{16\pi^2(1+\delta_{\Omega,0})}}[D^{J*}_{M,\Omega}(\phi_R,\theta_R,\phi)+p(-1)^J D^{J*}_{M,-\Omega}(\phi_R,\theta_R,\phi)]. \tag{14}$$

M and Ω are the quantum numbers for the projections of the total angular momentum on the space-fixed and body-fixed z-axis, respectively. The diatomic vibrational eigenfunctions, $\chi_v(r)$, are solutions of

$$\left\{-\frac{\hbar^2}{2\mu}\frac{\partial^2}{\partial r^2}+V_{BC}(r)-E_v\right\}\chi_v(r)=0. \tag{15}$$

Insertion of Eq. (13) into the time-dependent Schrödinger equation using the Hamiltonian, Eq. (12), yields a set of first order differential equations for the $\Phi^{JM}_{\Omega,v}(R,\theta,t)$ coefficients

$$i\hbar\frac{\partial\Phi^{JM}_{\Omega,v}(R,\theta,t)}{\partial t}=\sum_{\Omega',v'}\left\{\delta_{\Omega,\Omega'}\delta_{v,v'}\left[-\frac{\hbar^2}{2m}\frac{\partial^2}{\partial R^2}+E_v+\left\langle\chi_v\left|\frac{1}{2\mu r^2}\right|\chi_v\right\rangle\mathbf{j}^2\right]+\delta_{v,v'}\times\left\langle W^{Jp}_{M\Omega}\left|\frac{l^2}{2mR^2}\right|W^{Jp}_{M\Omega'}\right\rangle+\delta_{\Omega,\Omega'}\times\langle\chi_v|V(r,R,\theta)|\chi_{v'}\rangle\right\}\Phi^{JM}_{\Omega',v'}(R,\theta,t). \tag{16}$$

The solution of the above equations is performed by representing the $\Phi^{JM}_{\Omega,v}(R,\theta,t)$ on finite grids for both R and θ

$$\Psi^{JM}(\mathbf{R},\mathbf{r},t)=\sum_{\Omega\geqslant 0}^{J}\sum_{v}\sum_{kn} W^{Jp}_{M\Omega}(\phi_R,\theta_R,\phi)\times\langle R_k\theta_n|\Phi^{JM}_{\Omega,v}(t)\rangle\sqrt{w_k}\chi_v(r). \tag{17}$$

A set of equidistant points, R_k, is chosen for the radial grid, and the radial kinetic term is solved using the Fast Fourier Transform method.[37] For θ, we use a set of Gauss-Legendre quadrature points, θ_n, with weights w_n. Using a Finite Basis Representation (FBR) for the Euler angles and a Discrete Variable Representation (DVR) for θ is convenient since the interaction potential only depends on θ. The action of the angular momentum operators on the wavepacket is best described as three steps. First, the wavepacket is transformed to the spherical harmonics basis set, $Y_{j\Omega}(\theta,0)$, through a DVR tranformation, $T^{\Omega}_{nj}=\sqrt{w_n}Y_{j\Omega}(\theta_n,0)$. Second, the matrix elements of the angular momentum operators are evaluated in the spherical harmonics basis set as,

$$\begin{aligned}&\langle Y_{j\Omega}|\mathbf{j}^2|Y_{j'\Omega'}\rangle=\delta_{\Omega,\Omega'}\hbar^2 j(j+1),\\&\langle W^{Jp}_{M\Omega}Y_{j\Omega}|l^2|W^{Jp}_{M\Omega'}Y_{j'\Omega'}\rangle\\&\quad=\delta_{\Omega,\Omega'}\hbar^2[J(J+1)+j(j+1)-2\Omega^2]\\&\qquad+\delta_{\Omega,\Omega'\pm 1}\hbar^2\sqrt{1+\delta_{\Omega,0}+\delta_{\Omega',0}}\\&\qquad\times\sqrt{J(J+1)-\Omega\Omega'}\sqrt{j(j+1)-\Omega\Omega'}.\end{aligned} \tag{18}$$

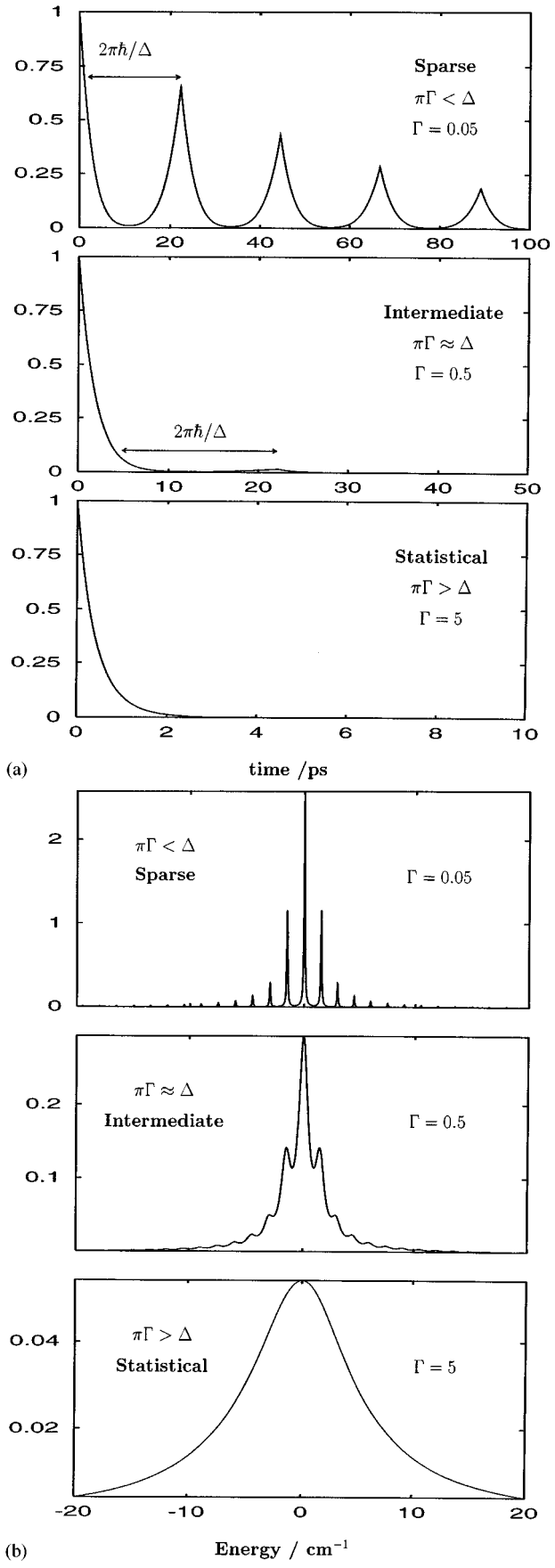

FIG. 1. Time evolution of the initial state (a) and spectrum (b) for the three IVR regimes. $\Delta=1.5$ cm^{-1} and $V=1$ cm^{-1} in all three cases. The values for Γ are in cm^{-1}.

The final expression is obtained by transforming back to the discrete variable representation. In practice, these three steps can be performed in a single operation,[38–42]

$$\mathbf{j}^2\langle R_k,\theta_n|\Phi^{JM}_{\Omega,v}\rangle(t)=\sum_{n'} A^{j}_{n',n}\langle R_k,\theta_n|\Phi^{JM}_{\Omega,v}\rangle(t), \tag{19}$$

$$\langle W^{Jp}_{M\Omega'}|l^2|W^{Jp}_{M\Omega}\rangle\langle R_k\theta_n|\Phi^{JM}_{\Omega,v}\rangle(t) = \sum_{n'} A^{\prime}_{n'\Omega',n\Omega}\langle R_k\theta_n|\Phi^{JM}_{\Omega,v}\rangle(t),$$

with

$$A^{j}_{n',n}=\sum_{j} \sqrt{w_{n'}}Y_{j\Omega}(\theta_{n'},0)\hbar^2 j(j+1)\sqrt{w_n}Y_{j\Omega}(\theta_n,0), \tag{20}$$

$$A^{\prime}_{n'\Omega',n\Omega}=\sum_{j} \sqrt{w_{n'}}Y_{j\Omega'}(\theta_{n'},0) \times\langle W^{Jp}_{M\Omega'}Y_{j\Omega'}|l^2|W^{Jp}_{M\Omega}Y_{j\Omega}\rangle\sqrt{w_n}Y_{j\Omega}(\theta_n,0).$$

In the body-fixed frame, it turns out that the only coupling between adjacent Ω components of the total wavepacket is due to the non-diagonal terms of l^2. This calculation is very well suited for massively parallel computing: each processor is assigned a value of Ω, and the exchange of information between processors is only due to the non-diagonal terms of l^2. $J=15$ calculations described in what follows were performed on a massively parallel computer. Test calculations for $J=1$, 3, and 7, showed that the CPU time per processor was independent of J.

This formalism provides a convenient set of zero-order quantum numbers, associated with H_0 of the IVR model, to describe both the initially excited wavepacket and its time development. The set of quantum numbers include v, describing the vibrational state of the free chlorine fragment; J, the total angular momentum; M, the projection of $\mathbf{J}$ on the space-fixed z axis; K, which orders the rotational sublevels of a given J, and is analogous to the asymmetric top K; p, the parity; and n, which characterizes the van der Waals vibrational level. In particular, H_0 is defined such that the discrete zero-order states are given by

$$\Phi^{JpMv}_{nK}(\mathbf{r},\mathbf{R})=\chi_v(r)\sum_{\Omega,j,m} a^{nK}_{j,\Omega,m}W^{Jp}_{M\Omega}(\phi_R,\theta_R,\phi) \times Y_{j\Omega}(\theta,0)\varphi_m(R), \tag{21}$$

where $\varphi_m(R)$ are radial basis set functions. For the case of $ArCl_2$ studied here, there is a further simplification in that the dipole allowed transitions from the ground vibrational level of the ground electronic state go to the ground van der Waals vibrational level, $n=0$, of a given vibrational level v of Cl_2. Thus the bright state wavepacket at $t=0$ is defined by choosing values for v, J, M, K, and p, and by setting $n=0$ in Eq. (21).

The autocorrelation function

$$c(t)=\langle\Psi^{JM}(t=0)|\Psi^{JM}(t)\rangle \tag{22}$$

gives the time dependence of the initial state population and the absorption spectrum is given by the Fourier transform of the autocorrelation function

$$\sigma(E) \propto \frac{1}{2\pi\hbar}\left[\int_0^\infty e^{iEt/\hbar} c(t)dt + \text{C.C.}\right]. \tag{23}$$

A particularly interesting quantity is the amount of energy stored in the Cl_2 stretching vibration as a function of time. This is evaluated by projecting the wavepacket onto the chlorine basis

$$P_v(t) = \sum_{\Omega} \int dR \int d\ \cos\ \theta |\langle \chi_v | \Psi^{JM}(\mathbf{R},\mathbf{r},t)\rangle|^2. \tag{24}$$

For the dissociative vibrational channels, $P_v(t)$ approximately gives the time dependence for the production of the final vibrational state v and can be directly compared with real time experiments.[5,6]

As in our previous studies of the IVR in $ArCl_2$, an atom-atom Morse potential is used to describe the short range part of the van der Waals attraction, $V(r,R,\theta)$ in Eq. (12), between the Ar and the Cl_2. The Morse parameters, $D=106$ cm^{-1}, $R_e=3.9$ Å and $\alpha=1.8$ $Å^{-1}$, are chosen to reproduce the experimentally determined bond energy, bond length,[13] and to approximately reproduce the time scale of the dynamics.[15] An anisotropic van der Waals form is used in the asymptotic region.[13] The Cl_2 potential, V_{BC} in Eq. (12), was obtained by a cubic spline interpolation of Coxon's RKR potential.[43]

For each case described in the next section, the exact time dependence and spectrum were calculated using Eqs. (22) and (23). The spectrum and time dependence were then fitted to the first-order model, Eqs. (6) and (7), using the smallest possible number of parameters. Finally, Eqs. (10) and (11) were used to characterize the regime of the IVR dynamics for each energy.

IV. RESULTS AND DISCUSSION

We have used the methods described in the previous sections to explore the effects of increasing vibrational and rotational excitation on the IVR dynamics of $ArCl_2$. The Cl_2 vibrational manifold is very anharmonic, as demonstrated by the dependence of the vibrational frequencies and rotational constants on v. This high anharmonicity allows us to explore different regimes of IVR by changing the quantum numbers of the molecule over a fairly small range. In particular, the number of vibrational quanta that must be transfered from the Cl_2 stretch to the van der Waals modes in order to dissociate the 178 cm^{-1} $ArCl_2$ bond changes quickly with v. For $1 \leqslant v \leqslant 7$, the transfer of only one quantum is necessary; for $8 \leqslant v \leqslant 16$, two quanta must be transfered; for $17 \leqslant v \leqslant 20$ three quanta; for $21 \leqslant v \leqslant 23$ four quanta and so on. We refer to these vibrational levels as the $\Delta v = -1$, -2, -3, and -4 regimes, respectively. For the higher vibrational levels, the Cl_2 vibrational quanta are much less than the $ArCl_2$ bond energy, and the dissociation process usually follows a sequential mechanism. Thus as v increases an increasing number of zero-order dark states are coupled and contribute to the dissociation dynamics.

In what follows, we examine one vibrational level from each Δv regime to observe how rapidly the number of states participating in the dynamics increases, and how strongly the states are coupled. For $\Delta v = -2$, we examine $v=10$; for $\Delta v = -3$, $v=18$; for $\Delta v = -4$, $v=22$; and for $\Delta v = -5$, $v=25$. In this part of the study, only $J=0$ states are considered. Over this range of v, the dynamics move from the sparse to the statistical regime.

Another way to go from the sparse to the statistical regime is through rotational excitation. Until recently such a study would have been too expensive computationally. The formalism we propose above for parallel computing makes it possible to study the rotational dependence in a reasonable amount of time. Our approach is quite similar to that recently described by Goldfield and Gray,[31] although they limited their study to $K=0$. One would expect that since the overall density of states is proportional to J, the dynamics should become more statistical as J increases. To explore this behavior, we have studied a variety of rotational levels for $v=18$. We find that the IVR regimes do not change qualitatively with J for the $K=0$ sublevels. Interestingly, however, for a given J, increasing K changes the IVR regime closer toward the statistical limit.

A. Increasing vibrational excitation, J=0

In this section, we discuss the effect of increasing vibrational excitation in the IVR dynamics. We examine one vibrational level for each Δv value greater than one.

1. v=10: minimum Δv=−2

The case of $v=10$ has been studied previously[13–15] in great detail using both the time-dependent and time-independent formalisms. This is a prototypical example of IVR in the sparse regime where a single dark state in the $v=9$ manifold mixes with the $v=10$, $n=0$ bright state to induce the dissociation to the $v=8$ continuum. Coherent excitation of the bright state results in an oscillation of the population between the bright and dark states as shown in Fig. 2(a). Since the dark state provides the doorway to the continuum, the dissociation flux follows the $v=9$ population, and the total $v=8$ population increases as a series of steps. The absorption spectrum in the region of the $v=10$ bright state is shown in Fig. 2(b). The two first-order states that share the bright state intensity are readily apparent in the figure. The non-exponential time dependence and the absorption spectrum are well reproduced by a fit to the first-order model, Eq. (4). In this case, the fit only requires two first-order states and one coupling term. The fit of the model to the exact calculation is also shown in Fig. 2. In the first-order model, the steps in the time dependence of the product appearance are clearly due to the Γ_{12} term which causes the interference between the two first-order states via the continuum. The two peaks of the absorption spectrum are also well reproduced by the analytical model.

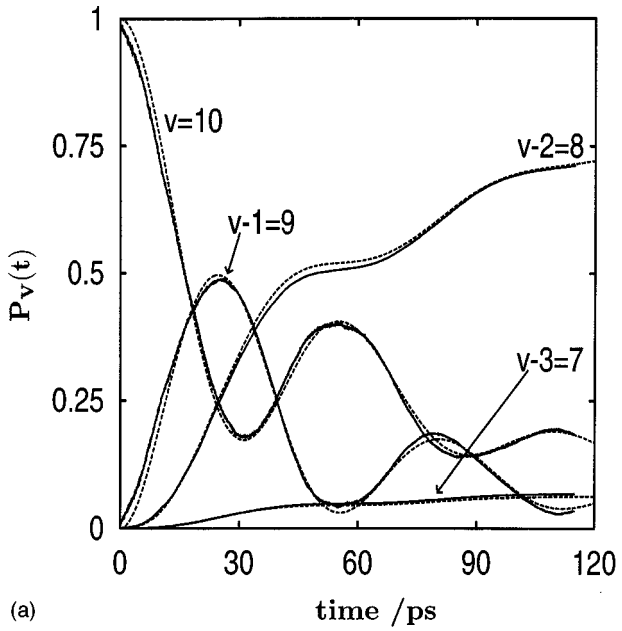

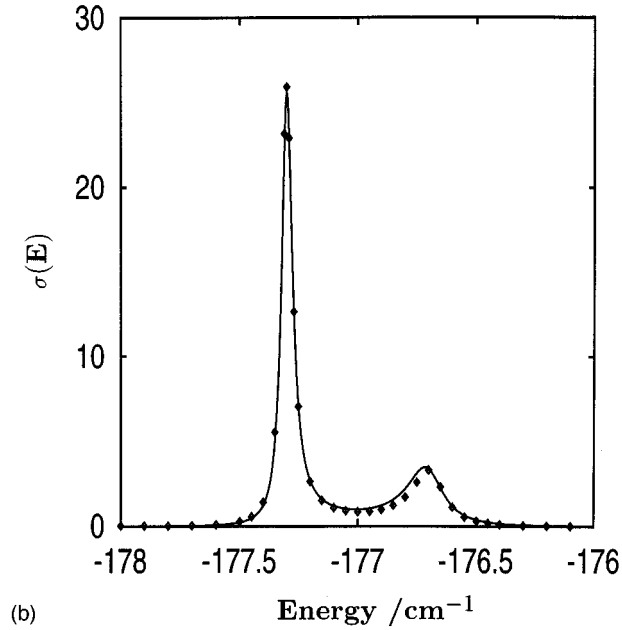

FIG. 2. Vibrational populations as a function of time (a), and absorption spectrum (b) for initial $v=10$ and $J=0$. The solid lines are the results of the wavepacket calculation, while the dashed lines correspond to the analytical fit in terms of independent resonances.

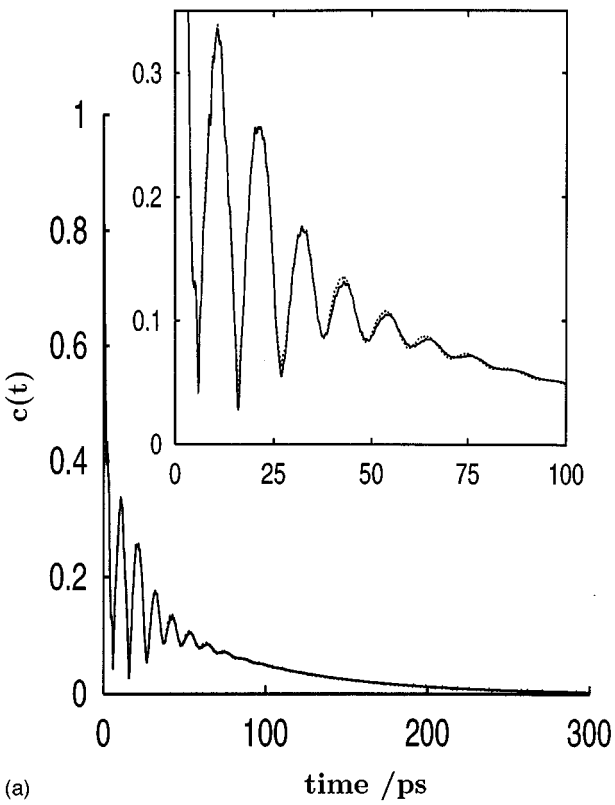

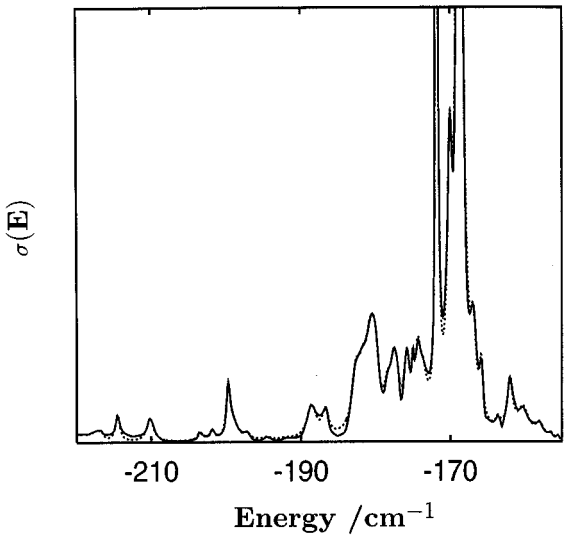

FIG. 3. Norm of the autocorrelation function as a function of time (a), and spectrum (b), for initial $v=18$ and $J=0$. The solid lines are the results of the wavepacket calculation, while the dashed lines correspond to the analytical fit in terms of independent resonances.

2. $v=18$: minimum $\Delta v=-3$

For $v=18$, for which the first open dissociation channel is $\Delta v=-3$, the results of the exact calculation and the first-order model are shown in Fig. 3. The nature of the absorption spectrum changes dramatically between $v=10$, Fig. 2(b), and $v=18$, Fig. 3(b). While the $v=10$ spectrum consists of the bright state and a single, well separated dark state, the $v=18$ bright state intensity is spread among a large number of dark state resonances forming a blended band about 20 cm^{-1} broad. In spite of the large number of states that contribute to the spectrum in the region of $v=18$, the autocorrelation function, Fig. 3(a), still shows a well defined beat pattern which indicates that the bright state interacts most strongly with one, or just a few, of the dark states before the population spreads into the rest of the manifold. Fig. 3 also shows the result of a fit of the exact spectrum to the first-order IVR model summarized by Eqs. (6) and (7). The fit requires 50 first-order states, although the bright state still accounts for 20% of the total intensity and the four most intense states carry 62% of the intensity. That this model,

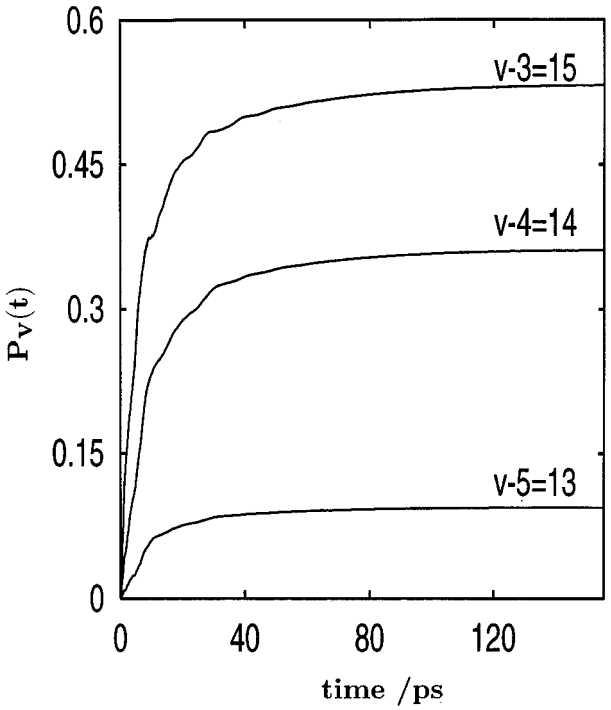

FIG. 4. Vibrational population of the dissociative channels of the Cl_2 fragment as a function of time for initial $v=18$ and $J=0$.

which incorporates an independent resonances assumption, works so well to fit the exact results indicates that when the number of doorway states is high, terms of the type Γ_{ij} $(i \neq j)$ are negligible as expected. This was one of the key assumptions in formulating the model.

The first-order model allows us to interpret in some detail the decay of the $v=18$ bright state resonance. The dynamics can be divided into three regions, based on timescale. For the shortest times, a few picoseconds, fast decay is due to a manifold of broad resonances. Several recurrences occur in the intermediate time regime, 10–50 ps. These are mainly due to the influence of the 4 narrowest resonances which account for 62% of the total intensity. These well separated resonances give a ''sparse regime'' character to the overall decay of the state. The long time decay is dominated by the single narrowest resonance, $E=-170$ cm^{-1}, $\Gamma=0.076$ cm^{-1} which accounts for 20% of the total weight of the state. This resonance is, of course, also very influential for the decay dynamics in the intermediate regime. If we calculate $\pi\Gamma/\Delta$ from the average values of the widths and spacings between adjacent resonances, the result is 0.7. This indicates that the overall decay occurs in the intermediate-sparse regime.

Even though the $v=18$ bright state must decay via a series of doorway states to the $\Delta v \geqslant -3$ manifold of final states, we have shown that its dynamics still have the character of the sparse regime, since the initial state vibrational population shows recurrences due to 4 main resonances. However, the population in the dissociative channels $v=15$, 14, and 13, increases nearly monotonically with time as shown in Fig. 4. This is closer to the behavior described by the model of independent resonances in Eq. (8). Therefore time-resolved experiments, which measure the appearance of the dissociated fragments of the complex, will be characteristic of the intermediate regime. This is not contradictory since the initial and final states are no longer directly connected but the dynamics proceed via a longer series of doorway states. Also, the probability of higher Δv processes increases dramatically in this regime of IVR. $\Delta v=-4$ accounts for 36% of the products and $\Delta v=-5$ for 10%. These values are considerably higher than what would occur in the sparse regime, except close to a resonance in the continuum when one channel is close to threshold.[15] In this regime it would be especially useful to have both time resolved data for the dissociation probability versus time and energy resolved experimental data for the absorption spectrum. Together, these two types of data would provide a detailed characterization of the dynamics of the state.

3. $v=22$: minimum $\Delta v=-4$

The autocorrelation function and spectrum for the $v=22$ bright state for which the minimum value of Δv is -4, are shown in Figs. 5. Compared to the $v=18$ spectrum, Fig. 3, the $v=22$ spectrum, Fig. 5(b), more closely corresponds to an envelop about 50 cm^{-1} broad that is not dominated by individual transitions. Also, the autocorrelation function, Fig. 5(a), decays very rapidly, with little regularity in the weak oscillations. In this case the fit to the independent resonances model includes 60 independent resonances. Although the number of resonances that must be included in the model does not increase dramatically over the $v=18$ case, the intensity is spread more evenly among the active resonances so that individual resonances are no longer so apparent. For $v=22$ the dynamics are clearly closer to the dense limit than for the lower levels, although the remnants of individual transitions are still visible. As the level of Cl_2 vibration increases, the number of coupled first-order states increases since more intermediate states are involved in the dissociation path. Also, the coupling between the states increases because of the greater anharmonicity. Using averaged values for Γ and Δ, $\pi\Gamma/\Delta=1.7$. This is 2.5 greater than the value for $v=18$. It is interesting to note that this increase is due more to a higher average value of Γ than to a lower average value of Δ. This confirms the interpretation that the move toward the intermediate regime is due more to a stronger coupling between states than to a higher density of states.

The evolution toward the statistical limit is also apparent in the final vibrational state population of the diatomic fragments, presented in Fig. 6. More vibrational states of Cl_2 are significantly populated than for the previous cases. As the IVR process approaches the statistical limit, more vibrational quanta get transfered to translation so that the final energy distribution of the fragments gets closer to a statistical distribution. It is very interesting that the population of the v-4 channel ($v=18$) goes through a maximum at $t=7$ ps and then decays (Fig. 6). This is a threshold effect. The spectrum is broad enough so that some dark state energies are above the opening of this product channel, and some are below. For

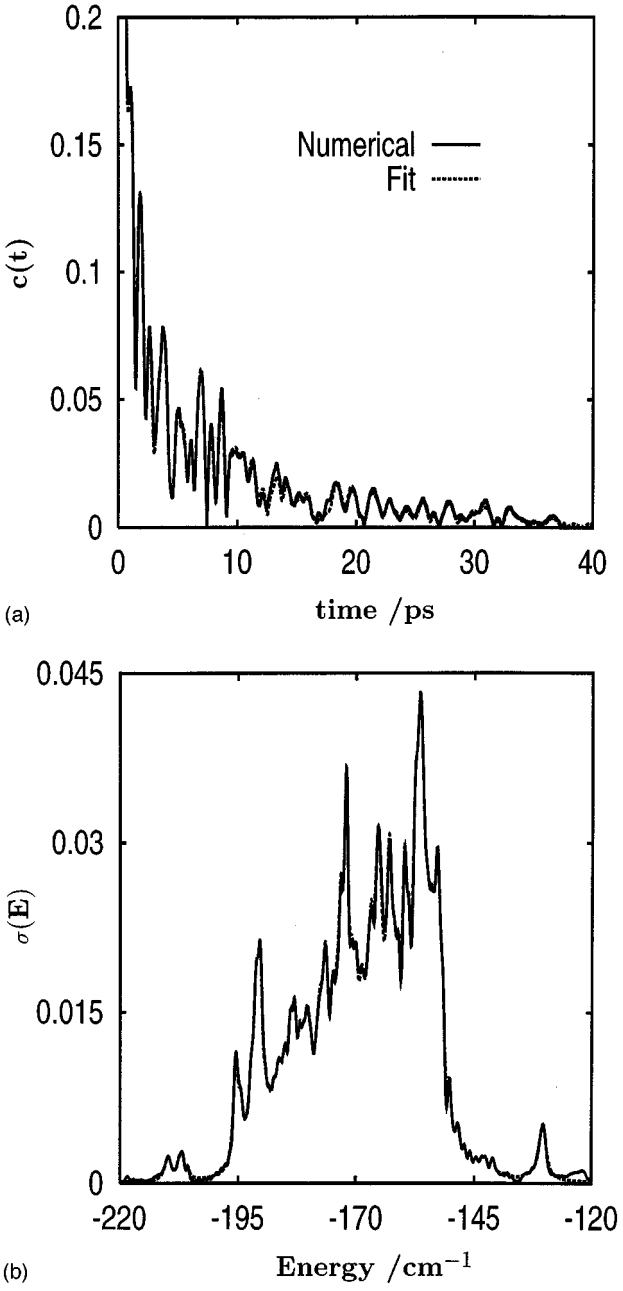

FIG. 5. Norm of the autocorrelation function as a function of time (a), and absorption spectrum (b), for initial $v=22$ and $J=0$. The solid lines are the results of the wavepacket calculation, while the dashed lines correspond to the analytical fit in terms of independent resonances.

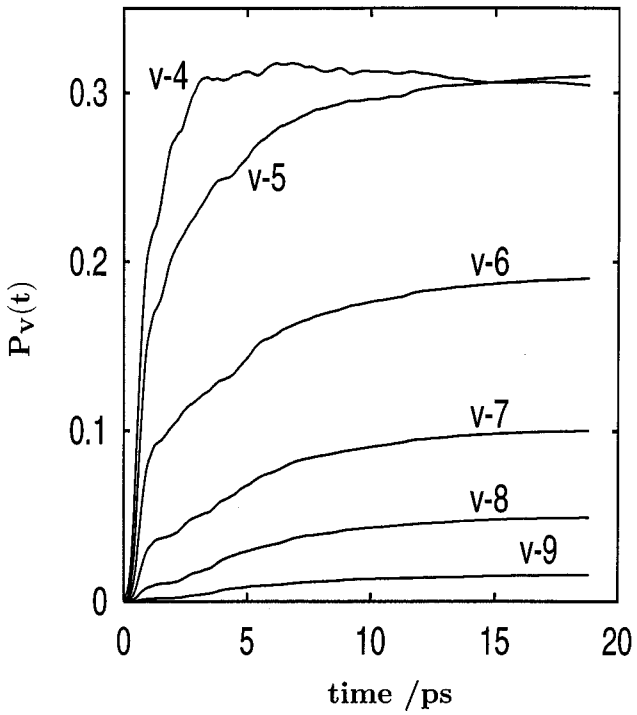

FIG. 6. Vibrational population of the dissociative channels of the Cl_2 fragment as a function of time for initial $v=22$ and $J=0$.

the later set of energies, the v-4 channel serves as a doorway to the v-5 continuum, so they become populated quickly, and decay slowly.

4. $v=25$: minimum $\Delta v=-5$

The spectrum and autocorrelation function for $v=25$, for which the minimum value of Δv is -5, are shown in Fig. 7. In this case, the time dependent approach did not converge, and the spectrum was obtained by numerically integrating the close-coupling equations[12,13] for solving the time-independent Schrödinger equation. As expected, the spectrum is even more congested than for $v=22$, the overall band being about 75 cm^{-1} broad. The fit to the independent resonance model in this case requires 86 resonances, with the most intense resonance contributing only 5% of the total. The autocorrelation function shown in Fig. 7(a) was obtained from this fit. The average values of Δ and Γ yield a value of $\pi\Gamma/\Delta=1.2$. In this sense the IVR dynamics for $v=25$ are slightly ''less dense'' than those of $v=22$. Although the density of states has continued to increase, the coupling appears to have leveled off. This could be partly due to the fact that although the Cl_2 stretch has a very large amplitude in this region, the frequency is getting to be rather low. Another fact that must be considered is that for this very high level, the quantum calculations may not quite be converged even though the basis contains 440 coupled channels distributed in 14 vibrational states. At this excitation the Cl_2, with a vibrational frequency only of the order of 20 cm^{-1}, is close to its dissociation energy.

The overall dependence of the $J=0$ spectra and decay curves for $ArCl_2$ vibrational predissociation depend on v about as expected. The IVR regime moves slowly away from the sparse toward the statistical regime as v is increased. Since $ArCl_2$ is only a triatomic molecule, however, the density of states does not increase dramatically, and even for $\Delta v=-5$ the dynamics have not reached the statistical limit.

B. Effect of overall rotation

When the VP process only requires $\Delta v=-1$, the decay rate seems to be rather independent of the total angular momenta considered. In the case where VP proceeds via IVR,

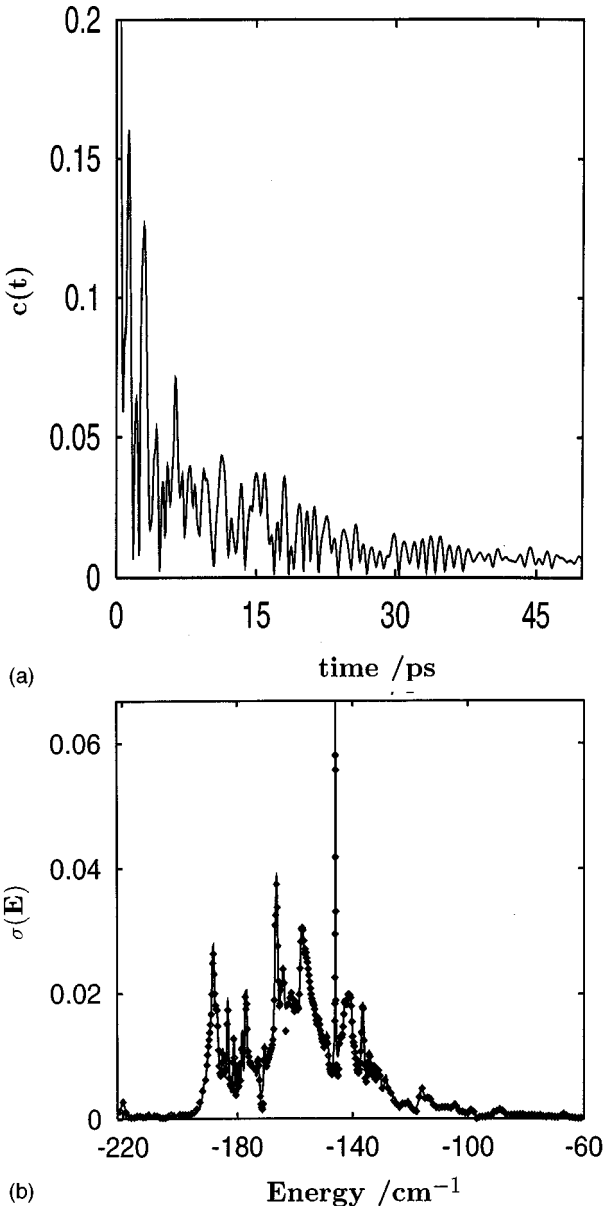

FIG. 7. Norm of the autocorrelation function as a function of time (a), and spectrum (b), for initial $v=25$ and $J=0$. The spectrum is the result of close-coupling time-independent calculations (Ref. 13), while the autocorrelation function was deduced from the analytical fit of (a) in terms of independent resonances.

the density of states for a system will obviously be greater if rotational excitation is included in the calculation. In many cases it has been shown that this also applies to the effective density of states (the density of ''active'' states, i.e., of states that are effectively coupled to the initial state) so that the dynamics of decay increases with rotational excitation. A previous study of ArI_2 appears to show that rotational excitation does not, however, cause a dramatic change in the dissociation rate for this molecule. In that study only states with $K=0$ were examined. Here we examine the effect of rotational excitation on the spectrum and dynamics of $ArCl_2$, $v=18$. In addition to examining the effect of increasing J, the total angular momentum, we also examine the effect of changing the orientation of the angular momentum among the molecular degrees of freedom (i.e., changing K). We chose the case of $v=18$ for closer examination because it is in the sparse-intermediate regime for which a change in the effective density of states might be expected to have the largest effect. Once the molecule is in the statistical limit, it would be expected that the IVR rate would be ''saturated'' and independent of J and K.

For very low values of J, Ω (the projection of J onto the intermolecular axis) is a reasonably good quantum number. However, as J increases, so does the Coriolis coupling; so that for higher values of J, (J,K) states become a mixture of more and more Ω components. In addition, Coriolis coupling is maximum for $\Omega=0$, since it is proportional to $\sqrt{J(J+1)-\Omega(\Omega+1)}$. As a consequence, it can be expected that the density of actively coupled states will increase with J, and that for a given J it will be maximum for $K=0$ (which is the state with the highest proportion of $\Omega=0$).

1. $K=0$, increasing J

Calculations performed for $J=1$ and 2 (with $K=0$) yield $\pi\Gamma/\Delta$ ratios of 0.83 and 0.87, respectively (instead of 0.69 for $J=0$). These higher values of the $\pi\Gamma/\Delta$ ratio are mainly due to an increase of $\langle\Gamma\rangle$, because the narrowest resonances become a little broader (see Fig. 8(a)). However, for all the J values studied, from $J=0$ to 15, the recurrences in the decay of the autocorrelation function persist. Hence even though the number of states increases, the coupling remains rather low and the effective density of states does not change appreciably. It is remarkable that the first recurrence is practically at the same position for all the values of J studied: 10.7 ps (for $J=0$) to 8.7 ps (for $J=15$). This corresponds to an energy spacing evolving smoothly with J from 3.1 to 3.8 cm^{-1}. The corresponding spectra show two main resonances with a spacing of 3.1 cm^{-1} for $J=0$, which smoothly increases with J. This effect has already been seen in time-independent calculations[14] and was interpreted as follows. If one of the resonances is mainly of ''bright'' character and the other mainly of ''dark'' character, the rotational constants for the quasibound state corresponding to the former are very close to the ones for the ground van der Waals level of the $v=18$ manifold, while for the latter they are very close to the ones for a very excited van der Waals level. Hence the energy of the quasibound states do not move by the same amount with J.

2. Increasing both J and K

We now turn to the effect of K, which characterizes the orientation of J with respect to the intermolecular axis, on the IVR process. First we vary K for the same J. The autocorrelation function for $J=7$ with $K=0$, 2, 4, and 6; $J=10$ with $K=0$ and 10; and for $J=15$ with $K=0$ and 14, are shown in Figs. 9. In nearly all the cases the recurrences persist, in particular the first one. However, it is clearly observed that for a given J, the amplitude of the recurrences strongly decreases with increasing K. In the case of $J=K=10$ the decay is nearly monotonic except for a reminis-

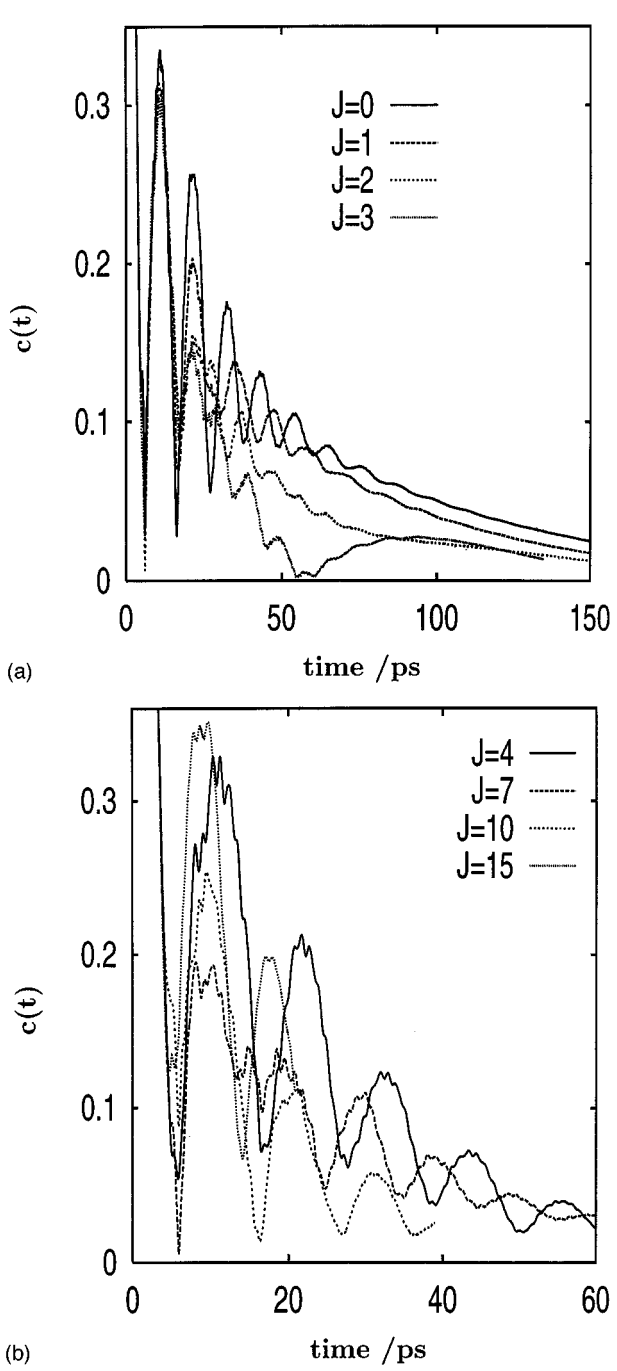

FIG. 8. $v=18$ autocorrelation function for (a) low values of J, (b) higher values of J, with $K=0$.

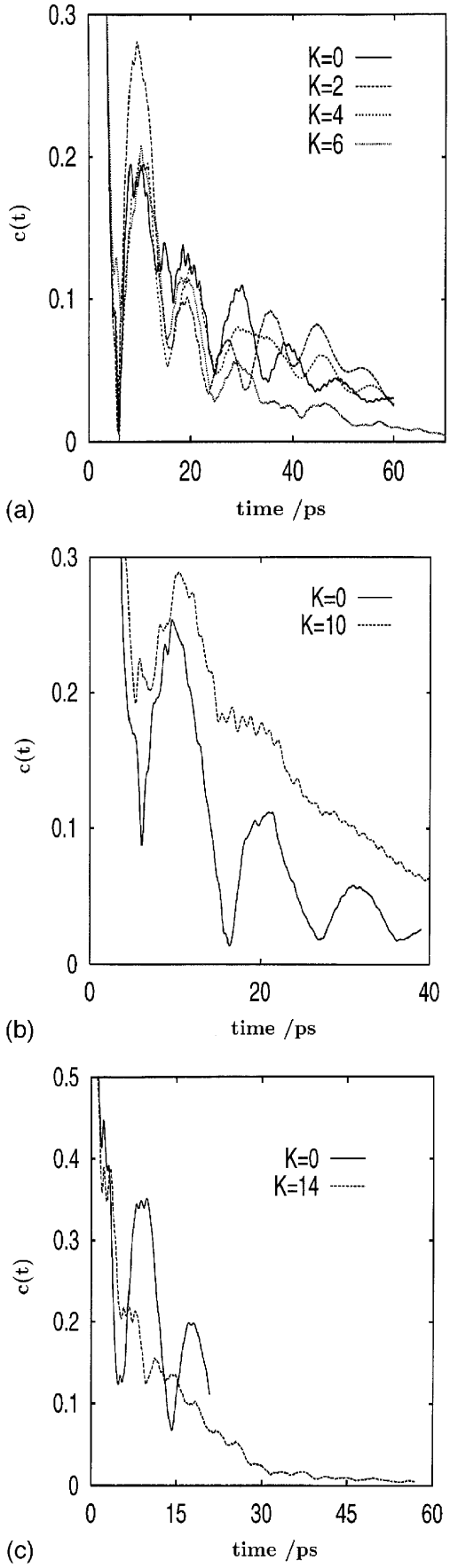

FIG. 9. $v=18$ autocorrelation function for (a) $J=7$, $K=0$, 2, 4, and 6, (b) $J=10$, $K=0$ and 10, and (c) $J=15$, $K=0$ and 14.

cence of the first recurrence at ≈ 10 ps. This recurrence nearly disappears in the case of $J=15$, $K=14$. For this case we continued the propagation long enough ($\approx$ 60 ps) to evaluate the absorption spectrum and the fit, in Fig 10, requires about the same number of independent resonances as was used for $J=0$, but now the $\pi\Gamma/\Delta$ ratio increases to 1.23. Therefore it may be concluded that in order to approach the statistical regime it is more important to increase K than J. This means that the Coriolis coupling is not directly responsible for the increase of ''active'' states. Instead, a less direct

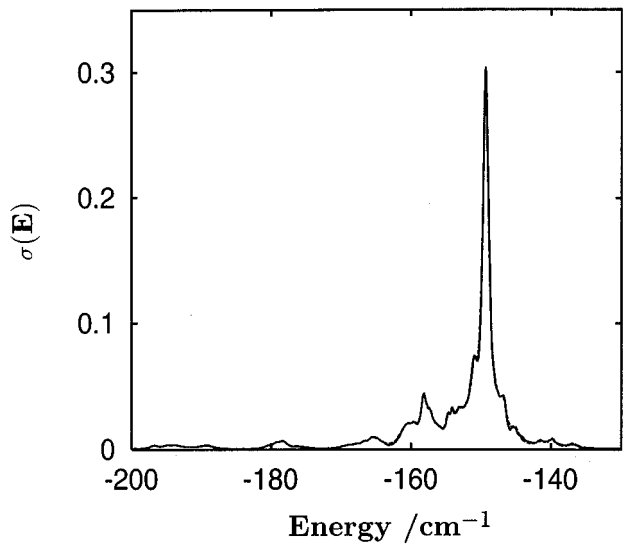

FIG. 10. Absorption spectrum for initial $v=18$, $J=15$, $K=14$.

effect is responsible of the increase of the density of active states with J. Indeed, Ω is not a good quantum number. However, only a few values of Ω centered around K are needed to describe the initial quasibound state. For $\Omega=0$, the matrix elements of the potential between angular basis functions is the same as for $J=0$. This is not the case for $\Omega\neq 0$. Classically, the difference between $\Omega=0$ and $\Omega=J$ is that $\Omega=J$ mainly corresponds to a rotation of the dihalogen molecule. For high values of Ω, since it is also the projection of **j** onto the intermolecular axis, this means that Cl_2 is rotating relatively fast, hence tends to stay perpendicular to **R**. This effect is also seen quantum mechanically, since the basis functions $Y_{j,\Omega=j}$ are more and more closely packed around the perpendicular configuration. Hence quasibound states with $\Omega=J$ are strongly affected by rotation while those with $\Omega=0$ are much less changed. A more careful study of this effect would be necessary in order to ascertain whether this is mainly due to the perpendicular equilibrium configuration of the complex.

C. Comparison with ArI_2

In addition to its fundamental interest, the vibrational predissociation dynamics in $ArCl_2$ may help clarify what happens in ArI_2. Several experiments[1,18,4,20] have revealed that for ArI_2 excited in the B electronic state of I_2, vibrational predissociation competes with electronic predissociation. Recently Burke and Klemperer[4] have measured the ratio of the electronic to vibrational predissociation rate constants for $16\leqslant v\leqslant 24$, where vibrational predissociation requires the transfer of 3 vibrational quanta of I_2 to the intermolecular bond. This ratio oscillates with v. From the fact that the ground and the first excited van der Waals levels had a very similar linewidth, they also deduced that the vibrational predissociation rate increases smoothly with vibrational excitation, which indicates that IVR occurs in the statistical limit. The measurements made by Zewail and coworkers[5,6] on the time dependence of the production of the $I_2(v-3)$ fragments for $v=18$ and 21 are compatible with this conclusion, as they show an exponential time dependence with a slightly higher rate for $v=21$ than for $v=18$. Hence the oscillations of the rate constant ratio were due to electronic predissociation and were attributed to the a state, because they were very similar to those observed in the electric-field induced quenching of $I_2(B)$ fluorescence.[44]

These oscillations of the electronic predissociation rate were well reproduced by a Golden Rule wave packet treatment.[45,46] However, recent calculations on the vibrational predissociation dynamics of ArI_2 (Refs. 22,23) have concluded that, for the potential surface used, IVR is in the sparse limit. This would give an erratic dependence of the VP rate with v for low J. The same conclusions were reached recently by Goldfield and Gray[31] for $J\gg 0$, although they did not examine the effect of the orientation of the total angular momentum with respect to the molecular system ($K=0$ in their calculations). Our work confirms these conclusions. However, the time dependence for the appearance of the Cl_2 fragments is very close to an exponential growth, as was seen in Fig. 4 for $v=18$ and Fig. 6 for $v=22$. Hence in the experiments measuring the production of the fragments as a function of time, it would be very difficult to differentiate between statistical and intermediate regime on the basis of this sole time dependence. To unambiguously characterize the IVR regime of a real system will require a combination of frequency-resolved and time-resolved spectroscopy, preferably for a system for which single state excitation is feasible.

More serious is the fact that the vibrational predissociation rate increases smoothly with vibrational excitation. Our work shows that for triatomic systems it is possible to reach an intermediate/statistical regime of IVR in which the VP rate constant would monotonically increase with v, if the rotational population of the complexes in the beam is taken into account. However, this is only true for certain orientations of **J** with respect to the molecular axes.

Another uncertainty concerning ArI_2 is the interaction potential, which is less well characterized than for $ArCl_2$. It is possible that a potential corresponding to a higher density of states in the middle to upper range of the well would bring the IVR dynamics closer to the statistical limit. Also, the strength of the coupling is well known to be very sensitive to the value of the range parameter of the Morse part of the potential, so that a small change might be expected to have a large effect on the IVR regime.

Finally, electronic predissociation may play a role in the IVR dynamics by giving a width to the dark states, therefore reducing the density of dark states necessary to obtain the statistical regime. This, together with the effect of the rotational angular momentum, could reconcile the experimental observations with the theoretical conclusions. Calculations are currently in progress to treat simultaneously electronic and vibrational predissociation.

V. CONCLUSIONS

In this study of IVR in $ArCl_2$ we have proposed an extension of the Bixon-Jortner model.[24] The active states are

prediagonalized to simplify the coupling scheme that must be considered, resulting in analytic expressions for the absorption spectrum and the time development of the states involved. This allows for an explicit determination of the average density of states and the average coupling strength for each initial excitation. We have demonstrated the utility of the new model by analyzing the dynamics of a variety of vibrational levels, which require the transfer of increasing number of quanta to effect dissociation. We have also examined the role of rotational excitation for the eighteenth Cl_2 stretching level. The ratio $\pi\Gamma/\Delta$ is useful for characterizing the regime of IVR for each initial level. The value of this ratio varies from much less than one in the sparse limit to much greater than one in the statistical limit.

As discussed previously, the $v=10$ level, for which the first open dissociation channel is $\Delta v=-2$, provides a prototypical example of IVR in the sparse regime. The initial bright state decays to the dissociation continuum by first coupling to a single doorway state in the $\Delta v=-1$ manifold. Two transitions (for $J=0$) appear in the spectrum since the doorway state borrows intensity from the bright state. The autocorrelation function of the initial excitation shows a well defined quantum beat structure due to the interference between these two states. This places the dynamics clearly in the sparse limit.

For higher initial vibrational levels, involving the transfer of three or more quanta of Cl_2 stretch, the active density of states is considerably higher, and the coupling between the active states also increases. The spectra for these states are heavily congested. The largest qualitative change occurs in going from $v=10$ to $v=18$. For $v=18$, 50 first-order states are required for a complete fit to the spectrum, but the four most intense transitions carry 62% of the total intensity. The autocorrelation function of the initially excited state shows a well defined beat pattern, with the amplitude of the first oscillation over 0.3. The value of the ratio $\pi\Gamma/\Delta$ is 0.7 for this transition. For $v=22$, 60 states must be included in the fit to the spectrum, only 10 more than for $v=18$. However, the intensity is much more evenly distributed so that the autocorrelation function decays rapidly with only low amplitude oscillatory structure. $\pi\Gamma/\Delta=1.7$, with most of the increase from $v=18$ due to increased coupling rather than increased density of states. The results for $v=25$ are not completely converged, but it appears that the dynamics for this level are less statistical than those for $v=22$: $\pi\Gamma/\Delta=1.2$. One possible explanation for this unexpected behavior is that the Cl_2 vibrational frequency for this level is quite low due to the large anharmonicity.

In addition, we have studied the role of the total angular momentum on the IVR dynamics for the case of $v=18$, which is in the intermediate regime for $J=0$. For low values of J, the ratio $\pi\Gamma/\Delta$ increases with J, since the density of levels increases with J, but not enough to make the recurrences of the autocorrelation function disappear. However, we have shown that varying the initial rotational sublevel K, corresponding to a different projection of the total angular momentum on the z body-fixed axis, Ω, has a more important influence on the dynamics. It is found that for $\Omega\approx J$, the process becomes closer to the expected behavior of the statistical limit. Varying experimentally the initially excited rotational sublevel,[7] should permit the analysis of this effect. The fact that the IVR dynamics evolve faster toward the statistical limit by increasing K for a given J rather than by increasing J for $K=0$ shows that Coriolis coupling is not directly responsible for this evolution. Instead, the move toward more statistical behavior must be due to changes in the van der Waals level wavefunctions, and/or to changes in the coupling between levels. These changes would then be more important for $K=J$, which has a large contribution of the rotation of the plane of the complex, than for $K=0$, where the complex rotates within a constant plane.

In this work values of J up to $J=15$ have been considered, which implies a number close to 6000 close-coupled equations in a time-independent calculations. However, using the time-dependent method with a mixed grid-basis representation for the angular coordinates was very appropriate for massively parallel computers. The calculations require almost the same real time for $J=15$ to run on sixteen processors than for $J=0$ to run on one processor.

This work clearly shows that due to the large anharmonicity of the Cl_2 stretch in the B electronic state, the IVR dynamics of $ArCl_2$ change rapidly from the sparse toward the statistical regime with increasing v. Perhaps surprisingly, we find that the change from sparse to statistical behavior has more to do with the increase in coupling than with the increase in the density of states, once a certain threshold density is obtained. This is especially true for rotational excitation. Increasing J, for $K=0$, has only small effects on the IVR dynamics, while increasing K for a given J has more dramatic effects. This shows that the increase in the number of coupled states due to Coriolis coupling is less important than might have been expected. The maximum values of $\pi\Gamma/\Delta$ that was observed, 1.7 for $v=22$, $J=0$ and 1.23 for $v=18$, $J=15$, $K=14$ are not yet at the statistical limit, but it would take a carefully crafted experiment to observe nonstatistical behavior for these levels. To accurately measure the regime of IVR for any level would require both frequency and time resolved spectroscopy, and some type of state selection to avoid initial state congestion.

The potential energy surface used for these calculations is reasonably accurate, and the results of these calculations are at least qualitatively correct. Similar calculations for ArI_2 have, so far, failed to indicate the onset of statistical behavior, in apparent contradiction to a growing body of experimental results. Unfortunately, the ArI_2 potential is much less well characterized than that of $ArCl_2$. Therefore, is important that the ArI_2 results be checked for sensitivity to the potential before too strong a conclusion be made regarding the apparent disagreements between experiment and theory.

ACKNOWLEDGMENTS

The authors would like to thank Pablo Villarreal and Alberto Beswick for intense and fruitful discussions. K.C.J. wants to thank the CNRS for financial support for an ex-

tended visit to Toulouse. N.H. thanks the French-Spanish collaboration fund ''Action Intégrée Picasso'' (AI96022) for a visit to Spain. This work has been supported by DGICYT (Spain) under Grant No. PB95-0071. We also want to acknowledge DGICYT and CIEMAT, for the use of a CRAY-J90, and CNRS, for the use of the parallel computing facilities (CRAY T3D) at IDRIS.

[1] D. H. Levy, Adv. Chem. Phys. **47**, 323 (1981).
[2] K. C. Janda, Adv. Chem. Phys. **60**, 201 (1985).
[3] R. L. Waterland, J. M. Skene, and M. I. Lester, J. Chem. Phys. **89**, 7277 (1988).
[4] M. L. Burke and W. Klemperer, J. Chem. Phys. **98**, 6642 (1993).
[5] D. M. Willberg, M. Gutmann, J. J. Breen, and A. H. Zewail, J. Chem. Phys. **96**, 198 (1992).
[6] M. Gutmann, D. M. Willberg, and A. H. Zewail, J. Chem. Phys. **97**, 8037 (1992).
[7] D. D. Evard, C. R. Bieler, J. I. Cline, N. Sivakumar, and K. C. Janda, J. Chem. Phys. **89**, 2829 (1988).
[8] J. I. Cline, D. D. Evard, F. Thommen, and K. C. Janda, J. Chem. Phys. **84**, 1165 (1986).
[9] D. D. Evard, F. Thommen, and K. C. Janda, J. Chem. Phys. **84**, 3630 (1986).
[10] J. I. Cline, N. Sivakumar, D. D. Evard, and K. C. Janda, Phys. Rev. A **36**, 1944 (1987).
[11] J. I. Cline, N. Sivakumar, D. D. Evard, and K. C. Janda, J. Chem. Phys. **86**, 1636 (1987).
[12] N. Halberstadt, J. A. Beswick, O. Roncero, and K. C. Janda, J. Chem. Phys. **96**, 2404 (1992).
[13] N. Halberstadt, S. Serna, O. Roncero, and K. C. Janda, J. Chem. Phys. **97**, 341 (1992).
[14] O. Roncero, P. Villarreal, G. Delgado-Barrio, N. Halberstadt, and K. C. Janda, J. Chem. Phys. **99**, 1035 (1993).
[15] K. C. Janda, O. Roncero and N. Halberstadt, J. Chem. Phys. **105**, 5830 (1996).
[16] D. G. Jahn, S. G. Clement, and K. C. Janda, J. Chem. Phys. **101**, 283 (1994).
[17] T. González-Lezama, M. I. Hernández, G. Delgado-Barrio, A. A. Buchachenko, and P. Villarreal, J. Chem. Phys. **105**, 7454 (1996).
[18] N. Goldstein, T. L. Brack, and G. H. Atkinson, J. Chem. Phys. **85**, 2684 (1986).
[19] M. L. Burke and W. Klemperer, J. Chem. Phys. **98**, 1797 (1993).
[20] K. E. Johnson, W. Sharfin, and D. H Levy, J. Chem. Phys. **74**, 163 (1981).
[21] S. K. Gray, Chem. Phys. Lett. **197**, 86 (1992).
[22] S. K. Gray and O. Roncero, J. Phys. Chem. **99**, 2512 (1995).
[23] O. Roncero and S. K. Gray, J. Chem. Phys. **104**, 4999 (1996).
[24] M. Bixon and J. Jortner, J. Chem. Phys. **50**, 3284 (1969).
[25] K. F. Freed and A. Nitzan, J. Chem. Phys. **73**, 4765 (1980).
[26] E. P. Wigner, Ann. Math. **53**, 36 (1951).
[27] Th. Zimmermann, L. S. Cederbaum, H.-D. Meyer, and H. Köppel, J. Phys. Chem. **91**, 4446 (1987).
[28] W. F. Polik, C. B. Moore, and W. H. Miller, J. Chem. Phys. **89**, 3584 (1988).
[29] H. S. Camarda and P. D. Georgopulos, Phys. Rev. Lett. **50**, 492 (1983).
[30] J. J. M. Verbaarschot, H. A. Weidenmüler, and M. R. Zirnbauer, Phys. Rep. **129**, 368 (1985).
[31] E. M. Goldfield and S. K. Gray, J. Chem. Soc. Faraday Trans. (to be published).
[32] T. Uzer, Phys. Rep. **199**, 73 (1991).
[33] W. H. Miller, Phys. Reports, **199**, 73 (1991).
[34] M. Bixon, J. Jortner, and Y. Dothan, Mol. Phys. **17**, 109 (1969).
[35] A. Nitzan, J. Jortner, and P. M. Rentzepis, Proc. R. Soc. London Ser. A **327**, 367 (1972).
[36] F. Lahmani, A. Tramer, and C. Tric, J. Chem. Phys. **60**, 4431 (1974).
[37] R. Kosloff, J. Phys. Chem. **92**, 2087 (1988).
[38] J. C. Light, I. P. Hamilton, and J. V. Lill, J. Chem. Phys. **82**, 1400 (1985).
[39] A. C. Peet and W. Yang, J. Chem. Phys. **91**, 6598 (1989).
[40] J. T. Muckerman, Chem. Phys. Lett. **173**, 200 (1990).
[41] G. C. Corey, J. W. Tromp, and D. Lemoine, *Numerical Grid Methods and Their Application to the Schrödinger Equation*, edited by C. Cerjan (Kluwer Academic, New York, 1993), p. 1.
[42] O. A. Sharafeddin and J. C. Light, J. Chem. Phys. **102**, 3622 (1995).
[43] J. A. Coxon, J. Mol. Spectrosc. **82**, 265 (1980).
[44] J. Tellinghuisen, J. Chem. Phys. **82**, 4012 (1985).
[45] O. Roncero, N. Halberstadt, and J. A. Beswick, Chem. Phys. Lett. **226**, 82 (1994).
[46] O. Roncero, N. Halbertadt, and J. A. Beswick, J. Chem. Phys. **104**, 7554 (1996).